Laser and Particle Beams

cambridge.org/lpb

Effect of pre-plasma on the ion acceleration by intense ultra-short laser pulses

Parvin Varmazyar, Saeed Mirzanejhad and Taghi Mohsenpour

Department of Atomic and Molecular Physics, Faculty of Basic Science, University of Mazandaran, Babolsar, Iran

Research Article

Cite this article: Varmazyar P, Mirzanejhad S, Mohsenpour T (2018). Effect of pre-plasma on the ion acceleration by intense ultra-short laser pulses. *Laser and Particle Beams* **36**, 226–231. https://doi.org/10.1017/S0263034618000241

Received: 23 December 2017
Accepted: 27 June 2018

Key words:
Laser foil interaction; PIC simulation; pre-plasma

Author for correspondence:
Parvin Varmazyar, Department of Atomic and Molecular Physics, Faculty of Basic Science, University of Mazandaran, Babolsar, Iran
E-mail: parvinvarmazyar@gmail.com, P.varmazyar@stu.umz.ac.ir

Abstract

In the interaction of short-laser pulses with a solid density target, pre-plasma can play a major role in ion acceleration processes. So far, complete analysis of pre-plasma effect on the ion acceleration by ultra-short laser pulses in the radiation pressure acceleration (RPA) regime has been unknown. Then the effect of pre-plasma on the ion acceleration efficiency is analyzed by numerical results of the particle-in-cell simulation in the RPA regime. It is shown that, for long-laser pulses ($\tau_p > 50$ fs), the presence of pre-plasma makes a destructive effect on ion acceleration while it may have a contributing effect for short-laser pulses ($\tau_p <$ 50 fs). Therefore, the 35 fs (20 fs) laser pulse can accelerate ions up to 40 MeV (55 eV), which is almost two (three) times larger in energy rather than use of a 100 fs pulse with the same pre-plasma scale length.

Introduction

The fast development of the laser technology has made the possibility of construction of super intense ($I > 10^{21}$ (W/cm^2)), high contrast (up to $\leq 10^{-14}$) (Braenzel *et al.*, 2015) and short-laser pulses (on order of several tens of fs) (Yang *et al.*, 2002; Waxer *et al.*, 2005; Lozhkarev *et al.*, 2006; Rus *et al.*, 2015) in recent years. Nowadays, ion acceleration driven by super intense laser pulses is one of the most interesting fields of research (Daido *et al.*, 2012) because of potential applications such as cancer therapy (Bulanov *et al.*, 2002; Malka *et al.*, 2004; Fourkal *et al.*, 2007), fast ignition (Roth *et al.*, 2001; Tajima and Mourou, 2002), ion imagining (Borghesi *et al.*, 2001, 2002) etc. Intense laser pulses, due to possessing very strong electric and magnetic fields, are capable of accelerating ions to high energies over very short distances (the acceleration gradients obtained in plasmas are 100–1000 GeV/m, orders of magnitude higher than 10–100 MeV/m typical values of conventional accelerators), allowing for what is called as a tabletop ion accelerator (Malka *et al.*, 2008; Malka, 2012).

In overdense plasma, depending on the laser parameters such as pulse duration, energy, intensity, and its polarization, and target properties such as density, species, and thickness, several mechanisms such as target normal sheath acceleration (TNSA) (Wilks *et al.*, 2001), radiation pressure acceleration (RPA) (Henig *et al.*, 2009), and shock wave acceleration (SWA) (Haberberger *et al.*, 2012) can create high energetic protons and ion beams. All of these mechanisms are based on production of a strong electrostatic field due to charge separation. Because of lower mass of electrons with respect to ions, electrons are pushed forward by the laser ponderomotive force, and the charge separation electrostatic field pulls ions forwardly.

Producing energetic protons and ion beams by irradiating high-power laser pulses on the target has been investigated in recent years (Dover and Najmudin, 2012; Wang *et al.*, 2014; Zhang *et al.*, 2015; Petrov *et al.*, 2016). Origin of accelerating protons is contaminant layers of water vapor or hydrocarbon behind the surface of target or oil. The early experiments indicate that the maximum energy ε_{max} of the accelerated protons scales with the laser intensity I and wavelength λ as $\varepsilon_{max} \propto (I\lambda^2)^{1/2}$ (Borghesi *et al.*, 2006; Fuchs *et al.*, 2006), consistent with the analytical model of TNSA.

The temporal structure of the laser pulse affects the laser–matter interaction and change the condition of the main pulse interaction with the target. The existing pre-pulse in laser pulse structure could ionize the front side of the target forming an expanding pre-plasma. Subsequent interaction of the main pulse with the target can be influenced by pre-plasma. Also, for long pulses (>100 ps), the main pulse itself can significantly takes place in the pre-plasma formation. Several techniques such as saturable absorbers (Itatani *et al.*, 1998) and polarization rotation in a hollow fiber (Homoelle *et al.*, 2002) before pulse stretching, plasma mirrors (Thaury *et al.*, 2007), and double chirped pulse amplification (Kalashnikov *et al.*, 2005) after pulse compression have been offered to modify temporal contrast of high-power lasers. Several experiments studied the effect of pre-plasma on generation and transportation electron and temperature of the hot electron generating by laser intensity (Lin *et al.*, 2012; Yang *et al.*, 2013). These experiments show that the spectrum, spatial distribution, and

CAMBRIDGE UNIVERSITY PRESS

divergence angle of the energetic electrons can be significantly changed in the presence of pre-plasma. Some experimental campaigns on the OMEGA-EP laser system show that the long-pulse length (of the order of ps) in conjunction with large initial pre-plasma has an impact on electron beam filamentation and creates multiple electron beams with large degrees of divergence (Peebles *et al.*, 2017). Shulyapov *et al.* showed that the acceleration efficiency of protons and multiply charged ions accelerated backwards under irradiation of the front surface of thick solid targets by high-power femtosecond laser radiation was determined by the contrast of this radiation (Shulyapov *et al.*, 2016). In the other work, experimental data represented that the presence of the pre-plasma leads to the decrease in the energy transfer efficiency of the laser beam to a solid target by fast electrons owing to the large divergence of streaming fast electrons which are generated far from the target surface (Pisarczyk *et al.*, 2015).

PIC simulation in order to determine the influence of pre-plasma on the proton energy has been investigated in the TNSA regime. It shows that at the optimum pre-plasma density gradient, dense relativistic electron bunches can be produced by the laser-driven ponderomotive channel. Then, this energetic bunch of electrons can reach behind the target and accelerate rear side protons efficiently (Zheng *et al.*, 2013). The influence of pre-plasma in the RPA regime of the ion acceleration was described by Liseykina *et al.* (2008). They presented an optimum scale for pre-plasma as $L_{pre} = 0.5\lambda$, for improvement of energy and efficiency of the acceleration in the RPA regime, but various scales for the laser pulse duration were not included in their analysis.

In this study, we focus on the effect of pre-plasma on the ion acceleration in the RPA regime when the laser pulses with different durations (of the order of several tens of fs) are irradiated on the target. We simulate interaction of high-power and short-laser pulses with thin the thickness of an aluminum target. Our simulation shows that the various laser pulse durations and pre-plasma scale lengths can affect ion energy. In the longer laser pulse regime ($\tau_p > 50$ fs), pre-plasma is undesirable and the energy exchange between the laser pulse and underdense plasma is destroyed by the coupling of the laser pulse with the cut-off layer. But for the shorter laser pulse duration regime ($\tau_p <$ 50 fs), an optimum value for the pre-plasma scale length is obtained, in which the ion energy increase considerably.

In Section "Interaction of short-laser pulse with an aluminum target", interaction of short-laser pulses with the aluminum target is demonstrated with the 1D3V particle-in-cell (PIC) code for four different pulse durations, $\tau_p = 20,\ 35,\ 100,\ 300$ fs. In Section "Pre-plasma effect", the effect of pre-plasma on the ion energy is demonstrated. Concluding remarks are given in Section "Conclusions".

Interaction of short-laser pulse with an aluminum target

To study the interaction of short-laser pulses with an aluminum target, the relativistic 1D3V PIC code (UMPIC)[1] is used. Our targets are thin foils ($L < 1$ μm) of pure aluminum with a density of 27 g/cc and an initial charge state of +10, dealing with the ionization processes by pedestal or pre-pulse, corresponding to an electron density of $n_e = 4.3n_c$. In the simulations, circularly polarized pulses with the same intensity ($I \sim 10^{21}$ W cm^{-2}, $a_0 = 15.2$) and wavelength ($\lambda_l = 0.8$ μm), but four different

[1]University of Mazandaran Particle-In-Cell simulation code.

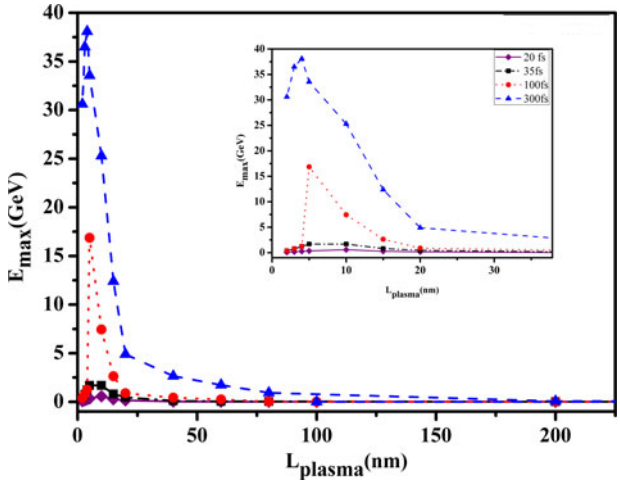

Fig. 1. Maximum ion energy as a function of target thickness without pre-plasma for different laser pulse durations $\tau_p = 20$ fs (purple solid line, diamonds), $\tau_p = 35$ fs (black dash-dotted line, squares), $\tau_p = 100$ fs (red dotted line, circles), and $\tau_p = 300$ fs (blue dashed line, triangles).

durations 20, 35, 100, and 300 fs are employed. The dimension of the foil changes from few nanometers to hundreds of nanometers, but the length of the interaction zone can be increased by a few micrometers due to the presence of pre-plasma.

In the simulations, the size of each cell and the equivalent time step are $\delta x = 6$ nm ($\simeq 0.0075\lambda_l$) and $\delta t \simeq 0.02$ fs, since $\tilde{\delta t} = \tilde{\delta x}$, where δx and δt are normalized cell length and time step, respectively. In each cell, 100 electrons and 10 ions are placed. Total interaction time is about 10 ns (~500 000 time steps), to cover all over the interaction area.

We first present the result of our simulations in the absence of pre-plasma (for very high contrast pulses). The maximum energy of ions as a function of target thickness is shown in Figure 1, for four different laser pulse durations. According to Figure 1, it seems that for targets with thicknesses more than 200 nm, different laser pulse durations almost deliver the same energy to the ions. In other words, for greater length foils, the increase of pulse duration is no longer effective on the ion acceleration. In contrast, maximum energy increases with decreasing target thickness up to an optimum thickness, which is obtained by the transparency condition of the thin foil (Bulanov *et al.*, 2016). Figure 1 (inset plot), shows that this optimum thickness increased with decreasing of the pulse duration. However, as one can see in Section "Pre-plasma effect", it cannot happen in reality, since in the real experiments, pre-pulse and pulse pedestal make a spatial pre-plasma profile that will clearly change recent results.

Regarding the phase space of the ions in Figure 2, it can be realized the involved ion acceleration regime. As one can see in Henig *et al.* (2009), in the RPA light sail regime the bulk of the target is displaced forward. For the thin foil targets (shorter than 200 nm), the dominant mechanism for the acceleration is RPA (Fig. 2a). It is clear in Figure 2b that for thick targets and shorter laser pulse duration, the TNSA mechanism can also appear behind the target.

Pre-plasma effect

In this section, we consider pre-plasma with a linear-density ramp in front of the foil. We assume the Maxwellian equilibrium

https://doi.org/10.1017/S0263034618000241 Published online by Cambridge University Press

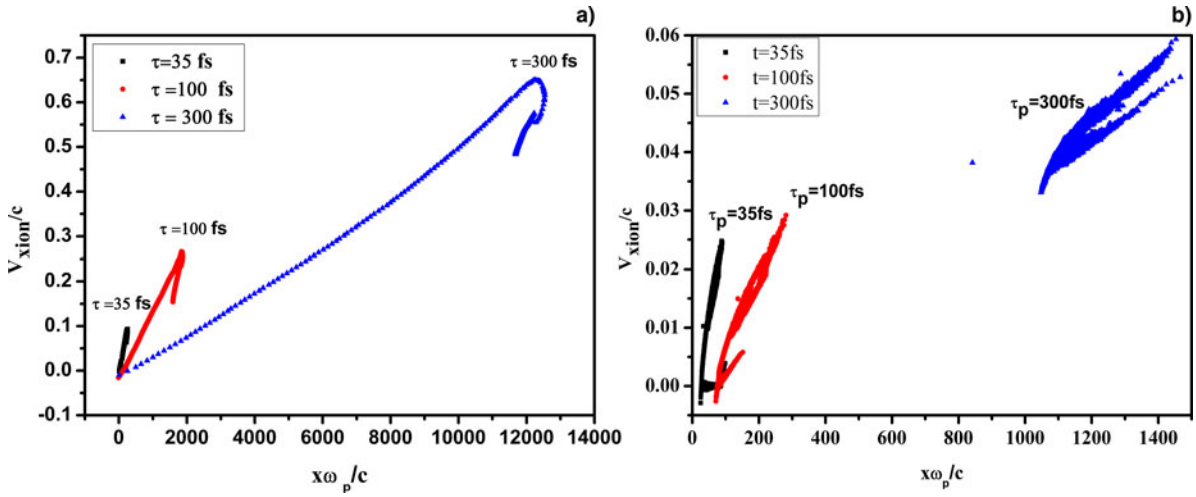

Fig. 2. Phase space of ions for two target thicknesses whithout pre-plasma: (a) $L_{plasma} = 40$ nm and (b) $L_{plasma} = 600$ nm.

distribution of electrons in the pre-plasma, with equivalent temperature, which is obtained by laser pulse ponderomotive potential (Haines *et al.*, 2009):

$$t_h \approx 0.47 a_{0p}^{2/3}, \tag{1}$$

where t_h is dimensionless temperature (it is dimensionless with the rest mass energy of an electron i.e. $m_0c^2 = 0.511$ MeV) and a_{0p} is dimensionless amplitudes of the electric field in the pre-pulse. This distribution of electrons propagates through the target and deposits its energy over stopping range R_0. As plasma is expanding in vacuum, a shock wave is formed and moves inside the cold plasma. According to Llor *et al.* (2015), there is a relationship between the electron energy ε_1 and depth of electron penetration z as follows:

$$\rho_0 z = \frac{2}{5}\frac{1}{S_0\varepsilon_0^{1/2}}\left(\varepsilon_0^{5/2} - \varepsilon_1^{5/2}\right), \quad S_0 = \frac{\pi e^4 Z \ln\Lambda}{m_i}, \tag{2}$$

where ε_0, S_0, and ρ_0, respectively, are initial energy, angular scattering, and density of an electron. Ze and m_i are charge and mass of plasma ions, respectively and $\ln\Lambda$ is the Coulomb logarithm. Then, stopping range is $R_0 = \rho_0 L_0 = (2\varepsilon_0^{1/2}/5S_0)$ where L_0 is the place that shock is formed. For our linear-density ramp of pre-plasma with the formula $\rho = \alpha z$ with $\alpha = (\rho_0/L_{pre})$ (L_{pre} is the pre-plasma length), we can find this stopping range as below:

$$L_0 = \sqrt{\frac{2L_{pre}}{\rho_0 S_0}}\varepsilon_0. \tag{3}$$

Therefore, stopping range changes for different lengths of pre plasma. It shows that for our selected parameters, stopping range for $L_{pre} = 1500$ nm is 420 nm which is almost coincident with the critical surface where laser pulse reflects from the target. Since, existing pre-pulse (or pedestal) in the temporal structure of the laser pulse creates pre-plasma on the target which is changing the interaction processes, we have chosen different intensity contrast ratio ($I_{Main\text{-}Pulse}/I_{Pre\text{-}Pulse}$) along with varying pre-plasma length from 5 nm to almost 1500 nm. Actually, different pre-plasma scale lengths may be obtained by various pre-pulse delays corresponding to the main laser pulse location. Figure 3 illustrates the maximum energy of ions as a function of pre-plasma length. Regarding Figures 3a and 3b, one can find an optimal pre-plasma thickness of ~1.5 μm for 20 and 35 fs laser pulses in order to take advantage of the maximum energy of ions. The decreasing of energy for larger values of L might be related to the weak coupling of the laser pulse with the cut-off layer (Liseykina *et al.*, 2008). As the figures show, for longer pulses optimum pre-plasma length declines and reaches zero. Of course, in the case of pulse durations of 100 and 300 fs, the weak crest occurs at 350 and 300 nm, respectively. In other words, the maximum energy of ions occurs when pre-plasma does not create on the target. Then for long pulse durations, the use of lasers with high enough contrast is necessary to reach more energetic ions, in spite of the short pulse duration which long pre-plasma help to acquire energy by ions. Therefore, the 35 fs laser pulse creates ~40 MeV ions, which is twice the energy of producing ions by the 100 fs pulse with the same pre-plasma scale length. As a consequence, it proposes that the real experiment use of laser pulses with short durations can resolve concerns about creating pre-plasma due to pre-pulse.

Our complementary simulation results show that for short-laser pulse ($\tau_p < 50$ fs), changing the target thickness along with the optimal pre-plasma length obtained from previous section cannot affect the ion acceleration significantly. But for the longer pulses ($\tau_p > 50$ fs), increasing target thicknesses decrease ion energy effectively. Figure 4 shows the maximum energy versus plasma length (a) for pulse duration $\tau_p = 20$ fs and optimum pre-plasma length 1500 nm and (b) for pulse duration $\tau_p = 100$ fs and optimum pre-plasma 350 nm.

In Figure 5(a), the simultaneous effect of the laser pulse duration and pre-plasma scale length is demonstrated in two-dimensional color graded image. It is shown that small pre-plasma scale length (high contrast pulse) is required for longer laser pulses ($\tau_p > 50$ fs), but large pre-plasma scale length has a suitable effect on shorter laser pulse ($\tau_p < 50$ fs).

Two suitable regions for ion acceleration are indicated in Figure 5(a), one for longer pulses without pre-plasma and the other for short pulse with pre-plasma. The advantages of the short-laser pulse region are smaller input energy and low contrast requirement. Also, Figure 5b shows relative conversion efficiency η/η_0 as a function of pulse duration and pre-plasma length (where

https://doi.org/10.1017/S0263034618000241 Published online by Cambridge University Press

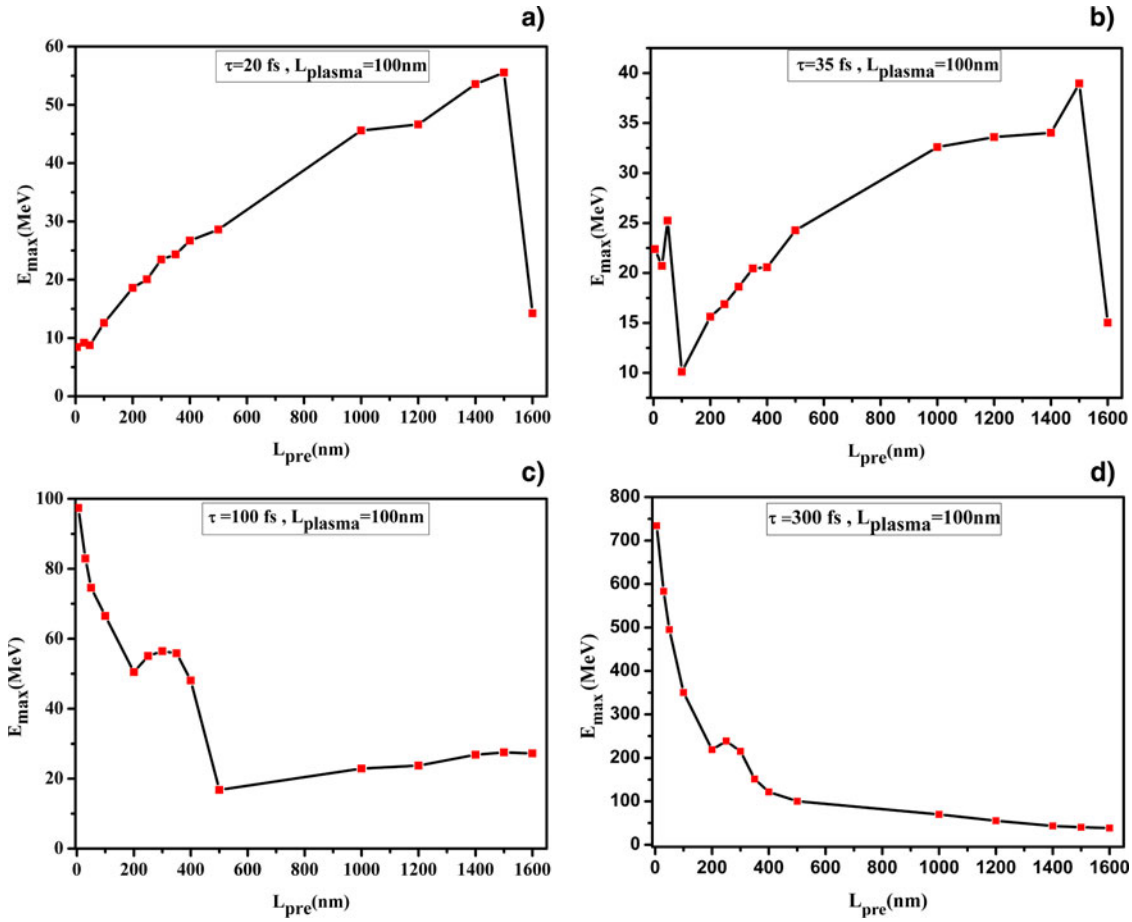

Fig. 3. Maximum ion energy as a function of pre-plasma thickness. For all diagrams, thickness of plasma is 100 nm. (a) $\tau_p = 20$ fs, (b) $\tau_p = 35$ fs, (c) $\tau_p = 100$ fs, and (d) $\tau_p = 300$ fs.

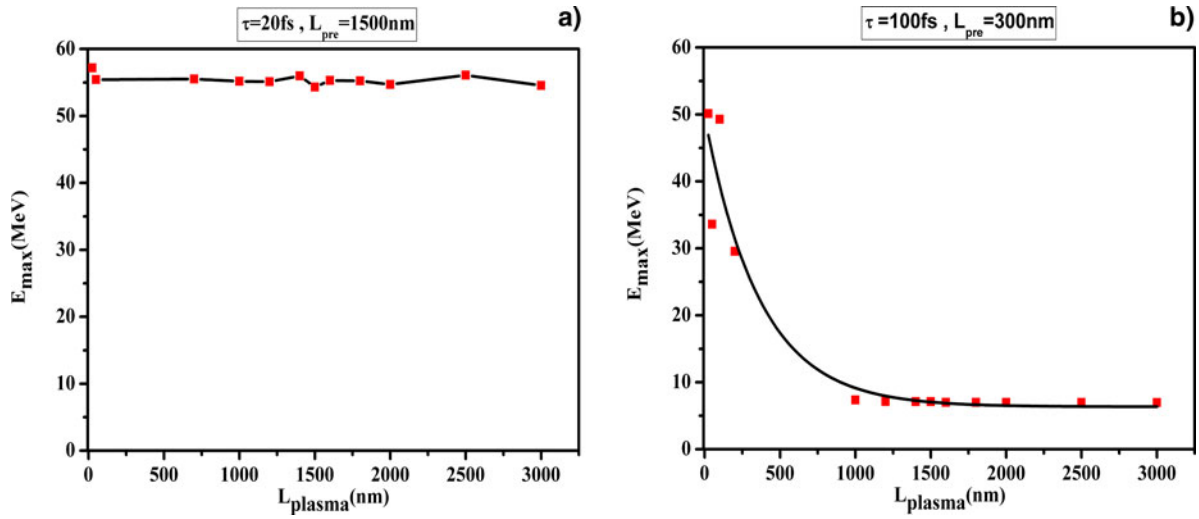

Fig. 4. Maximum energy versus plasma length: (a) for $\tau_p = 20$ fs, pre-plasma length is 1500 nm and (b) for $\tau_p = 100$ fs, pre-plasma length is 350 nm.

η is the efficiency of each pulse and η_0 is the efficiency of laser pulse with a duration of 20 fs and pre-plasma length of 1500 nm). As one can see, for longer pulses, relative efficiency decreases when pre-plasma length increases. Otherwise for shorter pulses ($\tau < 50$ fs), efficiency increases when pre-plasma scale length increases up to an optimum value. It indicates that by using short-laser pulses, efficiency of energy transport from the laser to ions increases and the laser contrast is less important.

https://doi.org/10.1017/S0263034618000241 Published online by Cambridge University Press

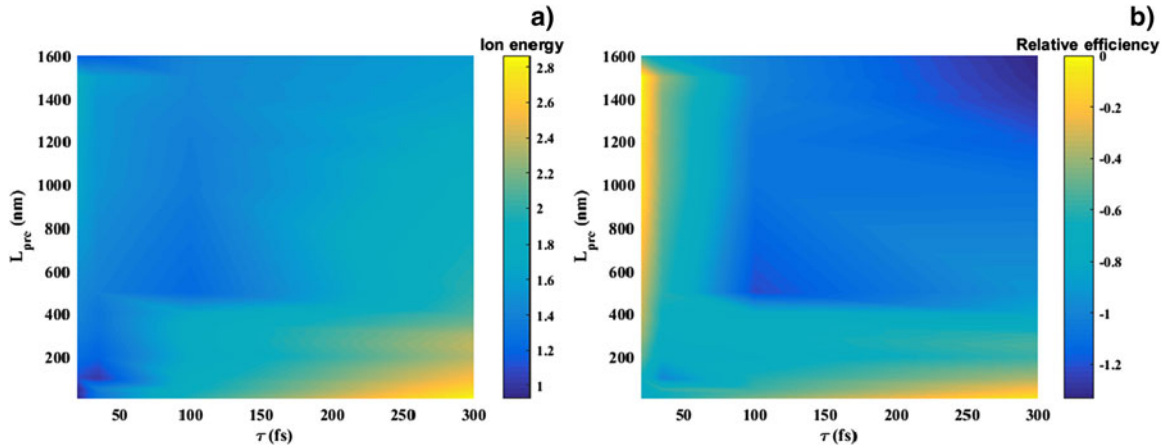

Fig. 5. (a) Ion energy (on logarithmic scale) as a function of pre-plasma length and laser pulse duration and (b) relative efficiency (η/η_0 on logarithmic scale) as a function of pre-plasma length and laser pulse duration.

Conclusions

Recent advances in the construction of high intensity and short-laser pulses, as well as the production of thin nanometer foils, have led to a dramatic increase in ion acceleration in the interaction of laser pulses with solid targets. However, it seems that high contrast laser pulses are required in order to achieve considerable results in the interaction of intense laser pulses with a nanometer-scale foil. In fact, the presence of pre-pulses can create pre-plasma with a given scale length, or even in the case of very thin foils, damage the foils before arrival of the main pulse. Our simulation results from the interaction of femtosecond laser pulses with pure aluminum nanoscale foils show that pre-plasma presence has a destructive effect on the acceleration process for long pulses, while for pulses shorter than 50 fs, pre-plasma with optimal length can have a desirable effect on ion acceleration. In other words, laser pulses with less energy and short durations can transfer considerable energy to the ions with suitable efficiency. For instance, in the interaction of laser pulse with $I \sim 10^{21}$ W cm^{-2}, $a_0 = 15.2$ and pulse duration 35 fs with a 100 nm foil along with 1.5 μm pre-plasma can create ions with energy up to 40 MeV, which is twice the energy of Al^{10+} ions for laser pulse with 100 fs duration with the same target structure. Therefore, it is not required to serve high-energy long pulses with high contrast pulses in order to achieve energetic ions in the interaction of laser pulses with the solid target. In contrast, use of longer pulses with low contrast may be affordable. It should be noted that long-laser pulse durations with high contrast ($\geq 10^{10}$) can create more energetic ions and more efficiency.

References

Borghesi M, Campbell DH, Schiavi A, Haines MG, Willi O, MacKinnon AJ, Patel P, Gizzi LA, Galimberti M, Clarke RJ and Pegoraro F (2002) Electric field detection in laser-plasma interaction experiments via the proton imaging technique. *Physics of Plasmas* **9**, 2214–2220.

Borghesi M, Fuchs J, Bulanov SV, Mackinnon AJ, Patel PK and Roth M (2006) Fast ion generation by high-intensity laser irradiation of solid targets and applications. *Fusion Science and Technology* **49**, 412–439.

Borghesi M, Schiavi A, Campbell DH, Haines MG, Willi O, MacKinnon AJ, Gizzi LA, Galimberti M, Clarke RJ and Ruhl H (2001) Proton imaging: a diagnostic for inertial confinement fusion/fast ignitor studies. *Plasma Physics and Controlled Fusion* **43**, A267–A276.

Braenzel J, Andreev AA, Platonov K, Klingsporn M, Ehrentraut L, Sandner W and Schnürer M (2015) Coulomb-driven energy boost of heavy ions for laser-plasma acceleration. *Physical Review Letters* **114**, 124801.

Bulanov SS, Esarey E, Schroeder CB, Bulanov SV, Esirkepov TZ, Kando M, Pegoraro F and Leemans WP (2016) Radiation pressure acceleration: the factors limiting maximum attainable ion energy. *Physics of Plasmas* **23**, 056703.

Bulanov SV, Esirkepov TZ, Khoroshkov VS, Kuznetsov AV and Pegoraro F (2002) Oncological hadrontherapy with laser ion accelerators. *Physics Letters* **A299**, 240–247.

Daido H, Nishiuchi M and Pirozhkov AS (2012) Review of laser-driven ion sources and their applications. *Reports on Progress in Physics* **75**, 056401.

Dover NP and Najmudin Z (2012) Ion acceleration in the radiation pressure regime with ultrashort pulse lasers. *High Energy Density Physics* **8**, 170–174.

Fourkal E, Velchev I, Fan J, Luo W and Ma CM (2007) Energy optimization procedure for treatment planning with laser-accelerated protons. *Medical Physics* **34**, 577–584.

Fuchs J, Antici P, d'Humières E, Lefebvre E, Borghesi M, Brambrink E, Cecchetti CA, Kaluza M, Malka V, Manclossi M and Meyroneinc S (2006) Laser-driven proton scaling laws and new paths towards energy increase. *Nature Physics* **2**, 48–54.

Haberberger D, Tochitsky S, Fiuza F, Gong C, Fonseca RA, Silva LO, Mori WB and Joshi C (2012) Collisionless shocks in laser-produced plasma generate monoenergetic high-energy proton beams. *Nature Physics* **8**, 95–99.

Haines MG, Wei MS, Beg FN and Stephens RB (2009) Hot-electron temperature and laser-light absorption in fast ignition. *Physical Review Letters* **102**, 045008.

Henig A, Steinke S, Schnürer M, Sokollik T, Hörlein R, Kiefer D, Jung D, Schreiber J, Hegelich BM, Yan XQ and Meyer-ter-Vehn J (2009) Radiation-pressure acceleration of ion beams driven by circularly polarized laser pulses. *Physical Review Letters* **103**, 245003.

Homoelle D, Gaeta AL, Yanovsky V and Mourou G (2002) Pulse contrast enhancement of high-energy pulses by use of a gas-filled hollow waveguide. *Optics Letters* **27**, 1646–1648.

Itatani J, Faure J, Nantel M, Mourou G and Watanabe S (1998) Suppression of the amplified spontaneous emission in chirped-pulse-amplification lasers by clean high-energy seed-pulse injection. *Optics Communications* **148**, 70–74.

Kalashnikov MP, Risse E, Schönnagel H and Sandner W (2005) Double chirped-pulse-amplification laser: a way to clean pulses temporally. *Optics Letters* **30**, 923–925.

Lin XX, Li YT, Liu BC, Liu F, Du F, Wang SJ, Chen LM, Zhang L, Liu X, Liu XL and Wang ZH (2012) Directional transport of fast electrons at the

https://doi.org/10.1017/S0263034618000241 Published online by Cambridge University Press

front target surface irradiated by intense femtosecond laser pulses with preformed plasma. *Laser and Particle Beams* **30**, 39–43.

Liseykina TV, Borghesi M, Macchi A and Tuveri S (2008) Radiation pressure acceleration by ultraintense laser pulses. *Plasma Physics and Controlled Fusion* **50**, 124033.

Llor Aisa E, Ribeyre X, Gus' kov S, Nicolaï P and Tikhonchuk VT (2015). Dense plasma heating and shock wave generation by a beam of fast electrons. *Physics of Plasmas* **22**, 102704.

Lozhkarev VV, Freidman GI, Ginzburg VN, Katin EV, Khazanov EA, Kirsanov AV, Luchinin GA, Mal'shakov AN, Martyanov MA, Palashov OV and Poteomkin AK (2006) 200 TW 45 fs laser based on optical parametric chirped pulse amplification. *Optics Express* **14**, 446–454.

Malka V (2012) Laser plasma accelerators a. *Physics of Plasmas* **19**, 055501.

Malka V, Faure J, Gauduel YA, Lefebvre E, Rousse A and Phuoc KT (2008) Principles and applications of compact laser–plasma accelerators. *Nature Physics* **4**, 447–453.

Malka V, Fritzler S, Lefebvre E, d'Humières E, Ferrand R, Grillon G, Albaret C, Meyroneinc S, Chambaret JP, Antonetti A and Hulin D (2004) Practicability of proton therapy using compact laser systems. *Medical Physics* **31**, 1587–1592.

Peebles J, Wei MS, Arefiev AV, McGuffey C, Stephens RB, Theobald W, Haberberger D, Jarrott LC, Link A, Chen H and McLean HS (2017) Investigation of laser pulse length and pre-plasma scale length impact on hot electron generation on OMEGA-EP. *New Journal of Physics* **19**, 023008.

Petrov GM, McGuffey C, Thomas AGR, Krushelnick K and Beg FN (2016) Generation of heavy ion beams using femtosecond laser pulses in the target normal sheath acceleration and radiation pressure acceleration regimes. *Physics of Plasmas* **23**, 063108.

Pisarczyk T, Gus' kov SY, Renner O, Demchenko NN, Kalinowska Z, Chodukowski T, Rosinski M, Parys P, Smid M, Dostal J and Badziak J (2015) Pre-plasma effect on laser beam energy transfer to a dense target under conditions relevant to shock ignition. *Laser and Particle Beams* **33**, 221–236.

Roth M, Cowan TE, Key MH, Hatchett SP, Brown C, Fountain W, Johnson J, Pennington DM, Snavely RA, Wilks SC and Yasuike K (2001) Fast ignition by intense laser-accelerated proton beams. *Physical Review Letters* **86**, 436.

Rus B, Bakule P, Kramer D, Naylon J, Thoma J, Green JT, Antipenkov R, Fibrich M, Novák J, Batysta F and Mazanec T (2015). ELI-Beamlines: development of next generation short-pulse laser systems. *Proceedings of SPIE* **9515**, 95150F.

Shulyapov SAE, Mordvintsev IM, Ivanov KAE, Volkov PV, Zarubin PI, Ambrožová I, Turek K and Savel'ev AB (2016) Acceleration of multiply charged ions by a high-contrast femtosecond laser pulse of relativistic intensity from the front surface of a solid target. *Quantum Electronics* **46**, 432–436.

Tajima T and Mourou G (2002) Zettawatt–exawatt lasers and their applications in ultrastrong-field physics. *Physical Review Special Topics – Accelerators and Beams* **5**, 031301.

Thaury C, Quéré F, Geindre JP, Levy A, Ceccotti T, Monot P, Bougeard M, Réau F, d'Oliveira P, Audebert P and Marjoribanks R (2007) Plasma mirrors for ultrahigh-intensity optics. *Nature Physics* **3**, 424–429.

Wang HY, Lin C, Liu B, Sheng ZM, Lu HY, Ma WJ, Bin JH, Schreiber J, He XT, Chen JE and Zepf M (2014) Laser-driven three-stage heavy-ion acceleration from relativistic laser–plasma interaction. *Physical Review E* **89**, 013107.

Waxer LJ, Maywar DN, Kelly JH, Kessler TJ, Kruschwitz BE, Loucks SJ, McCrory RL, Meyerhofer DD, Morse SFB, Stoeckl C and Zuegel JD (2005) High-energy petawatt capability for the OMEGA laser. *Optics & Photonics News* **16**, 30–36.

Wilks SC, Langdon AB, Cowan TE, Roth M, Singh M, Hatchett S, Key MH, Pennington D, MacKinnon A and Snavely RA (2001) Energetic proton generation in ultra-intense laser–solid interactions. *Physics of Plasmas* **8**, 542–549.

Yang X, Xu ZZ, Leng YX, Lu HH, Lin LH, Zhang ZQ, Li RX, Zhang WQ, Yin DJ and Tang B (2002) Multi-terawatt laser system based on optical parametric chirped pulse amplification. *Optics Letters* **27**, 1135–1137.

Yang XH, Ma YY, Xu H, Shao FQ, Yu MY, Yin Y, Zhuo HB and Borghesi M (2013) Generation of hemispherical fast electron waves in the presence of preplasma in ultraintense laser–matter interaction. *Laser and Particle Beams* **31**, 379–386.

Zhang H, Shen BF, Wang WP, Xu Y, Liu YQ, Liang XY, Leng YX, Li RX, Yan XQ, Chen JE and Xu ZZ (2015) Collisionless shocks driven by 800 nm laser pulses generate high-energy carbon ions. *Physics of Plasmas* **22**, 013113.

Zheng FL, Wu SZ, Zhang H, Huang TW, Yu MY, Zhou CT and He XT (2013) Preplasma effects on the generation of high-energy protons in ultraintense laser interaction with foil targets. *Physics of Plasmas* **20**, 123105.

https://doi.org/10.1017/S0263034618000241 Published online by Cambridge University Press